

www.acsami.org Research Article

Tribological Properties of Micropored Poly(2-hydroxyethyl methacrylate) Hydrogels in a Biomimetic Aqueous Environment

Yiwen Xi, Prashant Kumar Sharma,* Hans Jan Kaper, and Chang-Hwan Choi*



Cite This: ACS Appl. Mater. Interfaces 2021, 13, 41473-41484



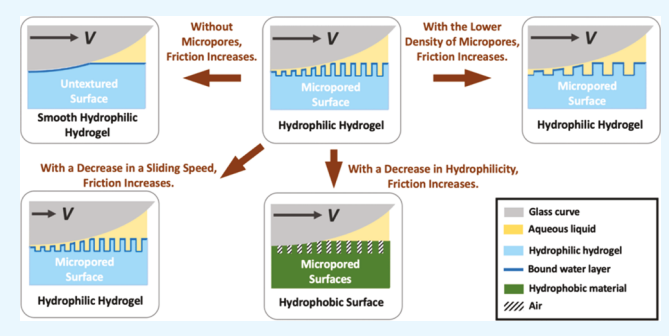
ACCESS I

Metrics & More

Article Recommendations

Supporting Information

ABSTRACT: The applications of hydrogels in tissue engineering as implants have rapidly grown in the last decade. However, the tribological properties of hydrogels under physiologically relevant conditions, especially those of textured hydrogels, have remained largely unknown due to the complexity of their mechanical and chemical properties. In this study, we experimentally investigated the tribological properties of micopored poly(2-hydroxyethyl methacrylate) (pHEMA) with the lateral pore dimensions varied compared to untextured pHEMA, the most commonly used hydrogel in ophthalmology, under physiologically relevant conditions. The pHEMA specimens were slid against a smooth glass curve under varying loads (6–60 mN, leading to an average



contact pressure of 10–21 kPa) and sliding speeds (1–10 mm/s) in phosphate-buffered saline (pH 7.4) at 33 °C to mimic the physiological conditions in human eyes. At relatively low loads and sliding speeds (e.g., 6 mN and 1 mm/s), the micopored pHEMA did not reduce the dissipated frictional energy significantly. However, at relatively high loads and sliding speeds (e.g., 60 mN and 100 mm/s), the micopored pHEMA resulted in significantly lower frictional energy (reduced by up to 68%) dissipation than the untextured pHEMA. The effect was more pronounced with the micropores with smaller dimensions. These are attributed to the greater amount and retentivity of the interfacial fluid supported by the free water squeezed out of the micropores with the smaller dimensions under the higher load and sliding speed. These results suggest that the use of micropore texturing on hydrogels in practice, such as for ocular applications, can be leveraged to reduce friction and wear under physiological conditions and hence lower the chance of inflammation near eye implants or keratoprosthesis.

KEYWORDS: biomaterials, hydrogel, tribology, microtextures, ophthalmology, tissue engineering

1. INTRODUCTION

Textured soft polymer materials have been gaining popularity in biomedical and tissue engineering applications. all the soft biomaterials, hydrogels, cross-linked polymer networks in an aqueous solution, have drawn notable attention in the recent decade. There are many advantages of using textured soft polymer materials in biomedical engineering applications, such as implants. Their similarity in mechanical properties to the human soft tissue (covering most of the surface on and inside the human body) with the addition of their biomimicking morphology can effectively improve cell growth including proliferation and differentiation. 4-6 Another advantage of using hydrogels, such as poly(2-hydroxyethyl methacrylate) (pHEMA) and poly-(ethylene glycol), is that their Young's moduli vary over a large range, that is, from a few kPa to a few MPa.⁷⁻⁹ Compared to hydrophobic biomaterials used in tissue engineering, such as polydimethylsiloxane (PDMS) and polyurethane with Young's moduli ranging from a few tens to hundreds of MPa, 10,11 hydrogel materials are soft and, because of their hydrophilicity, promote cell growth better.

The mechanical properties of hydrogel materials are often varied by changing their polymer concentration, that is, the mixing ratio between the polymer and crosslinker. The polymerization of hydrogels is usually initiated thermally by UV-irradiation or by a redox initiator system. The hydrogel surface is then typically textured through soft lithography such as through molding and imprinting processes performed during hydrogel polymerization. Although an increasing number of studies adopted microtexturing on hydrogel surfaces to manipulate cell growth, the tribological properties of microtextured hydrogels have not yet been well explored or understood. As suggested by the recent study on the tribological properties of micropored PDMS surfaces under physiological conditions, the sliding

Received: July 20, 2021 Accepted: August 16, 2021 Published: August 27, 2021





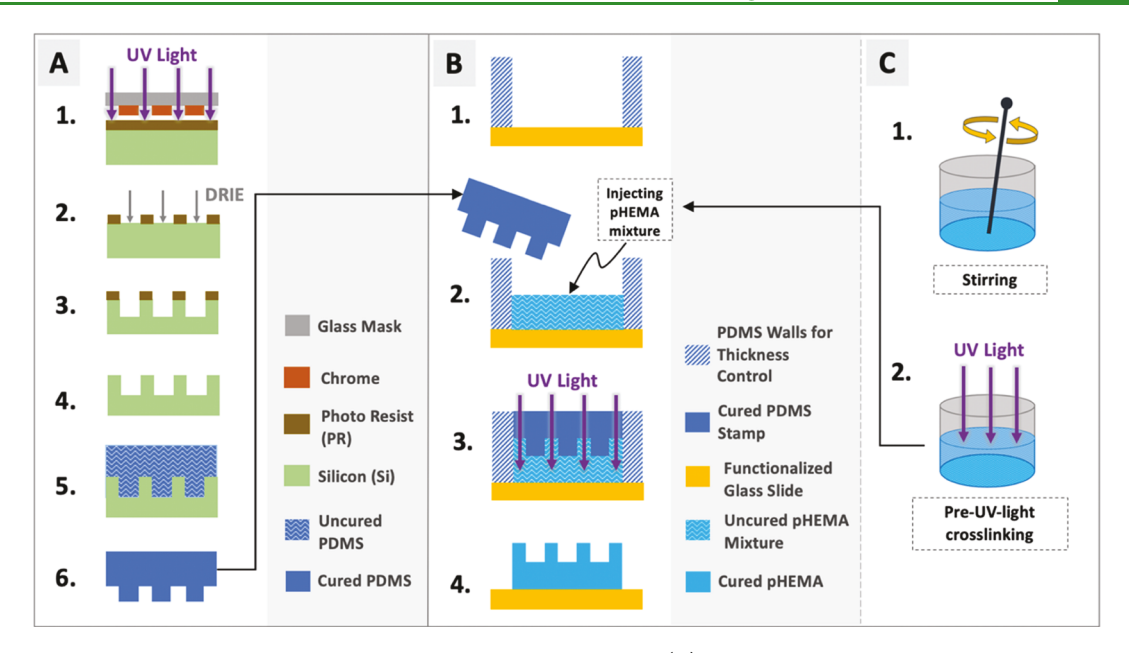


Figure 1. Schematic of the fabrication processes of micopored pHEMA films. (A) Preparation of a micropillared PDMS stamp: step 1 photolithography; step 2—DRIE of the silicon (Si) substrate; step 3—micropore patterns of Si obtained after DRIE; step 4—removal of the photoresist layer; step 5—casting of the uncured PDMS solution onto the Si mold; step 6—peeling off the solidified PDMS from the Si mold after curing. (B) Soft lithography process for the fabrication of micopored pHEMA films. (C) Preparation of the pHEMA solution under 1 min pre-UV light cross-linking.

interaction generated between the textured implant surfaces of soft materials and their biological surroundings can lead to an increase in friction and, hence, unnecessary or undesirable tissue wear. This can then eventually lead to superficial tissue damage to subsequent immune and wound healing responses along with patients' pain and discomfort. However, it should be noted that the soft polymer employed in the previous study—PDMS²—is a hydrophobic material. In many biomedical and tissue engineering applications, hydrophilic polymers such as hydrogels have also been widely used, such as in ocular applications. Compared to hydrophobic surfaces, textures on hydrophilic surfaces promote wetting and hydration.¹⁷ Moreover, compared to a nontextured smooth surface, the textured hydrophilic surfaces can help entrain the aqueous fluid into the sliding interface for lubrication and reduce the friction. For example, Etsion reported that micropore textures on hard materials such as steel could act as microreservoirs to lubricate the contact interface for bearing. 18-21 However, the tribological properties of soft textured hydrogel surfaces under physiologically relevant conditions have not yet been studied and reported in depth.

In this study, we investigate the tribological properties of microtextured hydrogel surfaces under physiologically relevant conditions. As for our hydrogel, we test pHEMA, the most commonly used hydrogel in ophthalmology. pHEMA was the first hydrogel recorded in the literature in 1960.²² With various monomers (e.g., polyvinyl pyrrolidone, monofunctional PDMS, and methacrylic acid) added, pHEMA-based hydrogels have been studied extensively for the application of contact lenses and keratoprosthesis in ophthalmology²³⁻²⁵ due to the biocompatibility and water content (~40%) of pHEMA.²⁶ As for the microtextures, we test micropore textures with their porosity and number density varied, to compare with the previous work that tested similar micropore textures for the hydrophobic polymer of PDMS.² In order to understand the tribological properties of micopored hydrogel surfaces under physiologically relevant conditions to ophthalmology, the coefficient of friction (COF) and the frictional force of both smooth (no textures) and micopored pHEMA surfaces are measured in phosphate-buffered saline (PBS, pH 7.4) at 33 °C in a reciprocating sliding motion (1-10 mm/s, which falls within the normal range of the average speed of the human eyelid during the closing and opening phases^{27,28}) against a hydrophilic glass curve to mimic the blinking of human eyes. Eyelid contact pressures are relatively low, usually ranging in 1-10 kPa; ²⁹⁻³¹ we apply a load to achieve contact pressures in a similar range. The total dissipated frictional energies, integrated as the friction force over the per-cycle sliding distance (2 × 10 mm), are compared between smooth and micopored pHEMA to develop a prediction of potential wear. Although both COF values and frictional energy are used to evaluate the tribological properties of the surfaces, the energetic approach of friction has the advantage of comparing the tests with varying durations in the dynamic motion, even when a steady state has not yet been achieved (i.e., under fretting, oscillatory, or unidirectional sliding conditions).32-We use the Hertzian contact theory to estimate the contact pressure and indentation depth during the tribological experiment, which are correlated to the measured data.

2. MATERIALS AND METHODS

2.1. Fabrication of Smooth and Microtextured pHEMA Films. Micopored pHEMA films were fabricated by using a soft lithography method, as illustrated in Figure 1. First, a micropillared PDMS stamp was prepared by cast molding (Figure 1A) and then used to create micopored pHEMA films by imprinting (Figure 1B). The detailed fabrication process is as follows. Ultraviolet (UV) photolithography (MA6 Mask Aligner, Suss MicroTec SE, Garching, Germany), followed by deep reactive ion etching (DRIE, Oxford Plasmalab 100, Oxford Instruments, Abingdon, UK), was first used to create micopored silicon (Si) molds, which would define the pore dimensions of the replicated pHEMA films with micropores (Figure 1A, steps 1-4). A self-assembled monolayer of perfluorodecyltri-

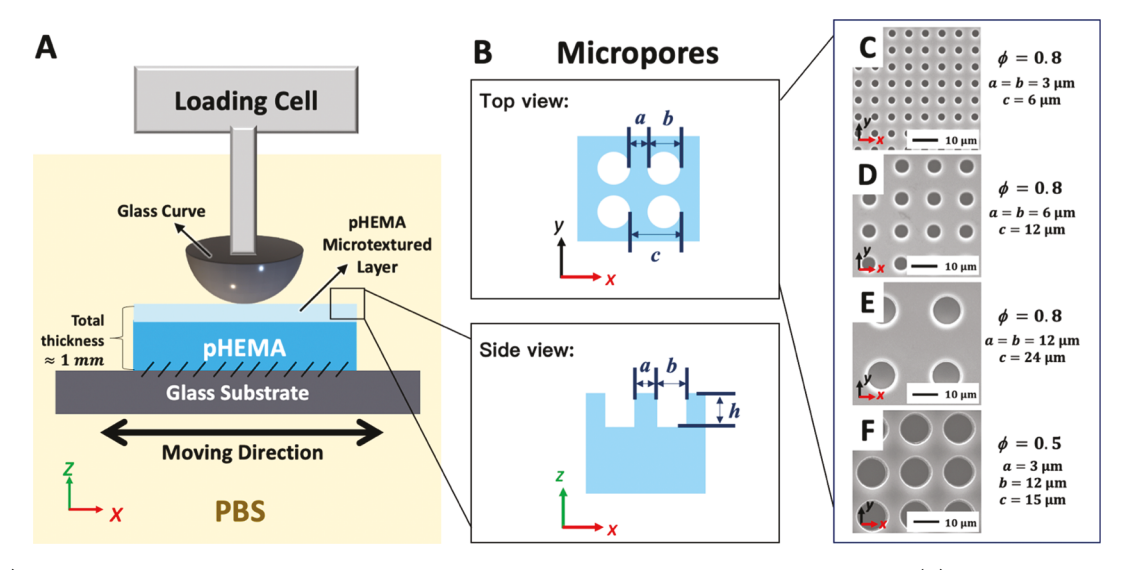


Figure 2. (A) Schematic of the measurement of the friction force and COF during the tribological experiments. (B) Schematic of the dimensions of the micropores of pHEMA films. While a, b, and c varied among the samples, h was constant to be 12 μ m. (C-F) Scanning electron microscopy images of the micropored silicon mold, which define the dimensions of the micropores of the pHEMA films replicated. ϕ is the solid area fraction defined as $\phi = \left[c^2 - \pi \left(\frac{b}{2}\right)^2\right]/c^2 = 1 - \frac{\pi}{4} \cdot \left(\frac{b}{c}\right)^2$.

chlorosilane (FDTS, Alfa Aesar, Haverhill, MA, USA), as an antiadhesive layer, was coated onto the Si mold by using molecular vapor deposition (MVD100E, Applied Microstructures, San Jose, CA, USA). After the mixture of the uncured PDMS monomer and its curing agent (10:1 in volume, Sylgard-184, Dow Corning, Midland, MI, USA) was cast over the FDTS-treated Si mold, the cast PDMS solution was exposed to vacuum at room temperature for 48 h for degassing until the PDMS was fully cured (Figure 1A, step 5). Afterward, the cured PDMS layer was peeled off from the Si mold (Figure 1A, step 6).

As for the pHEMA hydrogel, 5 mL monomer of HEMA (98%, Sigma-Aldrich, St. Louis, MO, USA) was mixed with 150 μ L of initiator (2-hydroxy-2-methylpropiophenone, 97%, Darocure-1173, Sigma-Aldrich, St. Louis, MO, USA) and exposed to UV light with an intensity of ~2000 mW/cm² (Spectrolinker XL-1500 UV crosslinker, Spectronics Corp., Westbury, NY, USA) for 1 min to first prepare an uncured pHEMA mixture (Figure 1C). Then, an additional 100 μ L of initiator and 50 μ L of crosslinker (ethylene glycol dimethacrylate, 98%, Sigma-Aldrich, St. Louis, MO, USA) were added into the mixture and were completely mixed, followed by degassing for about 30 min under less than 100 Torr in a vacuum chamber at room temperature (~25 °C).

Then, the uncured pHEMA mixture was poured into a PDMSwalled reservoir (the height of the walls: ~4 mm; the PDMS walls were prepared by the casting and curing processes on a bare silicon wafer) with a glass slide (25 mm \times 75 mm) at the bottom (Figure 1B, steps 1-2). The glass was functionalized with 3-(trimethoxysilyl)propyl methacrylate (TMSPMA, Sigma-Aldrich, St. Louis, MO, USA) to ensure a stable adhesion between the pHEMA hydrogel film and glass slide even when the hydrogel film is fully polymerized and subject to swelling in aqueous solution. As for the functionalization, each glass slide was covered with 20 μ L of TMSPMA for 20 min on one side, right after a 15 min UV-ozone treatment (UV.TC.220, Bioforce Nanosciences, Inc., Salt Lake City, UT, USA) in a fume hood. Then, the glass slide was placed onto a hotplate to be annealed at 100 °C for 30 min, followed by 110 °C for 10 min. After cooling down, the glass slide was rinsed with water and then ethanol thoroughly, followed by drying with compressed nitrogen (N2) gas. After the uncured pHEMA solution was poured into the reservoir, the micropillared PDMS stamp was carefully placed onto the solution and gently pressed down to make the pHEMA solution fully wet the PDMS stamp. To ensure that the pHEMA solution fills the micropillared PDMS stamp, the pHEMA solution was degassed

during the filling process for ~10 min in a vacuum chamber (pressure less than 100 Torr) at room temperature. Then, the pHEMA solution was exposed to UV light (intensity of $\sim 2000 \text{ mW/cm}^2$) for 45 min to finalize the polymerization of pHEMA (Figure 1B, step 3). In the end, the PDMS walls and the PDMS stamp were taken off to collect the cured pHEMA film adhered onto the glass slide (Figure 1B, step 4). Then, the pHEMA film was quickly rinsed with 70% ethanol followed by PBS (pH = 7.4) to remove unreacted chemical residues from the surface and to avoid dehydration. Before tribological tests, each pHEMA film, attached on the functionalized glass slide, was immersed in PBS at 4 °C for at least 24 h to allow the hydrogel to be fully swollen. A relatively tough elastic hydrogel, such as pHEMA, has a relatively low mesh size (<2 nm) and high polymer concertation. 35,36 Although the hydrophobicity of the PDMS stamp can lead to incompletely polymerized chains on the pHEMA surface (referred to as "heterogeneous hydrogel surface") and form dangling chains on a nanoscale on top of the pHEMA surface when fully hydrated, 37,38 the nanoscale chains should not influence the effect of the microscale textures (a pore diameter of 3000 to 12,000 nm with a pore depth of 12,000 nm) examined in this study because of the sizable difference in

A smooth (untextured) pHEMA film was also prepared in the same way except that a smooth PDMS stamp made by using a bare (polished) silicon wafer for cast molding was used instead of the micropillared PDMS stamp. A compression test was performed with the smooth pHEMA film by the universal microtribometer (UMT-3, Bruker, Billerica, MA, USA) to obtain an average Young's modulus of the bulk pHEMA (~1 mm in thickness) under contact pressures ranging from 9 to 177 kPa (for detail, see Supporting Information). The average Young's modulus of the smooth pHEMA of ~1 mm in thickness was 1.2 ± 0.1 MPa. The average Young's modulus was used for the calculation of the interfacial contact area and indentation depth using the Hertzian contact theory, as many others used the Hertzian contact theory to estimate the contact pressure, contact area, and indentation depth of pHEMA or pHEMA-based hydrogels. $^{39-41}$

2.2. Tribological Experiments. In the tribological experiments, the lateral friction force and the COF of the pHEMA films were measured using the UMT-3 in a reciprocating sliding mode, as illustrated in Figure 2A. Each specimen of the smooth and micopored pHEMA films of 1 mm in thickness, held on the functionalized glass substrate, was slid against a smooth glass curve (radius of 30 mm) at two different loads (F = 6 and 60 mN) and two different sliding speeds (V = 1 and 10 mm/s), respectively, in PBS (pH 7.4) at 33 °C

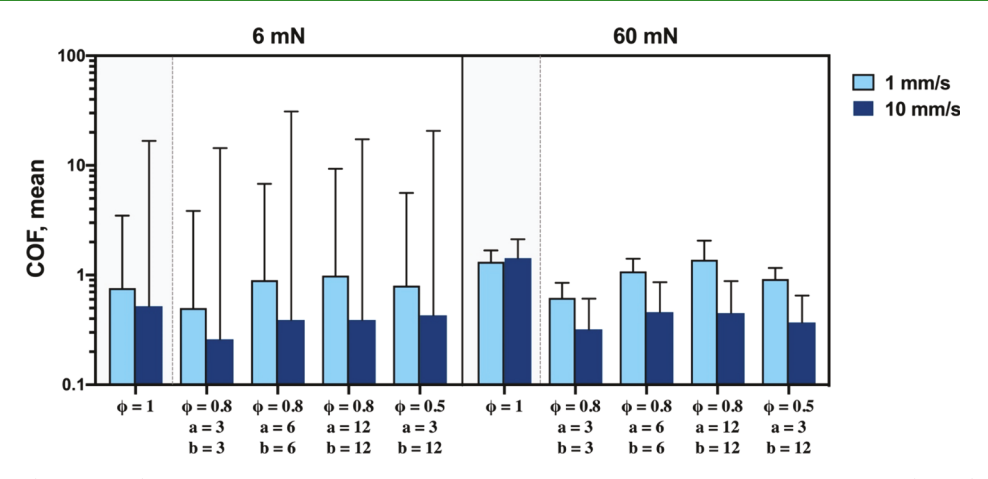


Figure 3. Mean COF (in log-scale) of the micopored pHEMA surfaces compared to that of the untextured pHEMA ($\phi = 1$) under two different loads (6 and 60 mN) and sliding speeds (1 and 10 mm/s). The error bars in the graphs represent standard deviations. (Statistical sample size: n = 200,000 for 1 mm/s; and n = 20,000 for 10 mm/s). Detailed results of the *t*-test analyses can be found in Supporting Information, Tables S4 and S5, for the effects of the dynamic conditions (load and sliding speed) and micropore texturing, respectively.

to mimic the conditions in human eyes. The pHEMA film was moved along the x-direction (shown in Figure 2A) back and forward over a sliding distance of 10 mm for 10 cycles during one tribological measurement at the given applied load and set sliding speed, sliding in total 200 mm (10 mm × 10 cycles × 2 directions) for one set of the experiment, where the sliding speed referred is the value set in the UMT-3; the actual sliding speed varies within each test cycle in the reciprocating mode, specifically when the motion direction was changed (see Figure S2 in Supporting Information for the examples of real-time velocity). Most tribological conditions in the human body are in such a reciprocating mode as the eyelid and knee joint movements. The period showing the acceleration of the loading cell ranged from less than 4% up to 30% of the total duration of each cycle for the set sliding speed ranging from 1 to 10 mm/s. The dissipated frictional energy was analyzed in addition to the COF in this study in order to account for the transient characteristics.

Both the pHEMA film and glass curve were immersed in the PBS solution at 33 °C throughout the whole experiment. The COF values and the frictional energy based on the measurement of the friction force data were used to evaluate the tribological properties of the smooth and microtextured pHEMA. The values of the friction force and the derived COF were collected using the UMT-3 with a measurement frequency of 1000 Hz. The raw data were analyzed using Python, which extracted the dissipated frictional energy and a mean COF value per sliding cycle. The dissipated frictional energy was calculated as a numerical integration of the friction force over one sliding cycle distance using the trapezoidal rule. An average of the frictional energy and the mean COF values of the middle eight cycles (i.e., discarding the first and last cycles showing unsteady behaviors due to the unstable loading conditions in the initial acceleration at the beginning of the 1st cycle and the final deceleration at the end of the 10th cycle) were used for data interpretation. Each experiment was repeated three times under the same conditions. Hence, the average of the frictional energy and the mean COF value of a total of 24 cycles (8 cycles × 3 times) for the given condition were finally used for statistical analysis. For statistical analysis, the two-way ANOVA with Tukey's multiple comparisons was used to analyze the frictional energy, whereas the t-test with assumed unequal variance for the sufficient statistical sample size (i.e., n > 20,000 in our case) was used to analyze the COF mean values due to the non-normal distribution of the COF raw data (based on the Kolmogorov-Smirnov normal test, which is a nonparametric test). A significant difference was assumed for p < 0.05 for both analyses.

For the micopored pHEMA films (Figure 2B), four different micopored samples, as shown in Figure 2C-F, were tested and compared to the smooth (untextured) one. In order to investigate the effect of the pore dimensions on the tribological properties, the

diameter of the pore (b) and the spacing between pores arranged in a square array (a) were varied concurrently from 3 to 12 μ m, while the solid area fraction (ϕ , a ratio of the top surface area to the projected area) was kept constant as $\phi=0.8$ (Figure 2C–E). In order to examine the effect of the solid area fraction on the tribological properties, the micropore pattern of $\phi=0.5$ (Figure 2F) was also tested, where the pore diameter ($b=12~\mu$ m) was much larger than the interpore spacing ($a=3~\mu$ m). For a smooth surface, $\phi=1$. The depth (h) of all the micropore patterns was constant at 12 μ m.

A smooth (roughness $R_a < \bar{S}$ nm, measured by the atomic force microscope; see Figure S3 in Supporting Information) glass curve with a radius of curvature of 30 mm was used to slide against each specimen of the smooth and microtextured pHEMA films during the tribological experiments. The glass curve was cut from a hollow glass sphere (manufactured by the University of Groningen Glass Blowing Shop) into a 5 mm \times 5 mm square piece having a thickness of 2 mm. Before the tribological experiments, the glass curve was washed by sonicating in RBS35 2% solution for 10 min, followed by soaking in ethanol for 10 min and rinsing with hot water and Milli-Q water three times, which ensured the cleanness and hydrophilicity of the glass curve

3. RESULTS AND DISCUSSION

3.1. Coefficient of Friction. As shown in Figure 3 (also see Tables S4 and S5 in Supporting Information for the t-test analysis), the result shows that the COF values of both smooth and micopored pHEMA surfaces are affected by the load and sliding speed, agreeing with other studies. ^{29,42–44} The increase in the sliding speed (from 1 to 10 mm/s) generally decreased the COF values under both 6 and 60 mN for all the surfaces, regardless of the microtextures on the surfaces, while the mean COF values lie within 0.1-1. The decrease in the COF with the increase in the sliding speed was more significant under a higher load of 60 mN with p < 0.0001 for all the surfaces. At a relatively low sliding speed of 1 mm/s, the COF values of all the surfaces increased significantly (p < 0.0001) with an increase in the load from 6 to 60 mN. However, at a relatively fast speed of 10 mm/s, only the COF value of the smooth surface ($\phi = 1$) increased significantly (p < 0.001). Under a relatively low load of 6 mN, only the micopored surface with the smallest pore and gap sizes ($\phi = 0.8$ with $a = b = 3 \mu m$) showed a significantly smaller COF value than the smooth surface (p < 0.0001) at a sliding speed of 1 mm/s; yet in the rest of the cases, micropore texturing with various dimensions did not reduce the COF; the micropore texturing either

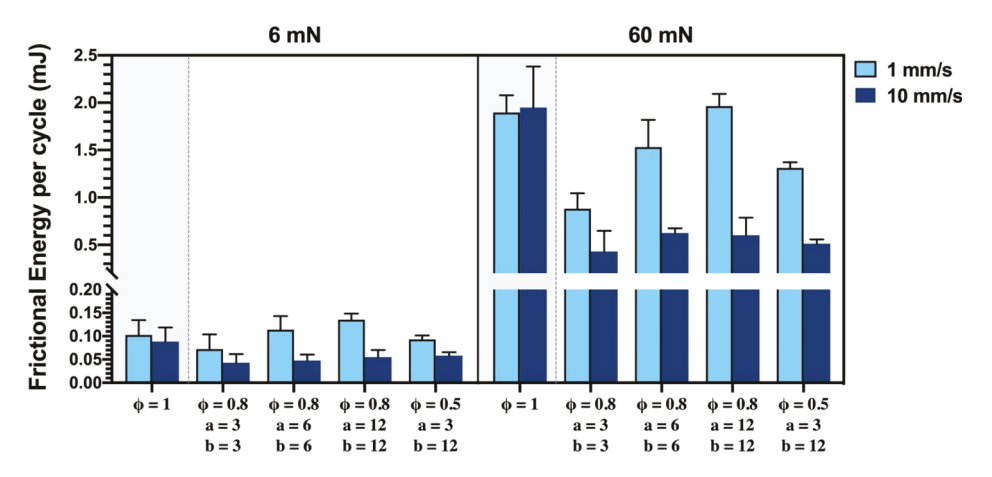


Figure 4. Dissipated frictional energy per cycle of glass-micopored pHEMA reciprocating sliding compared with that of the glass-smooth pHEMA $(\phi = 1)$ sliding under two different loads (6 and 60 mN) and sliding speeds (1 and 10 mm/s). The error bars in the graphs represent standard deviations (statistical sample size: n = 24). The results of two-way ANOVA analyses are shown in Tables 1 and 2 for the effects of the dynamic conditions (load and sliding speed) and the micropore textures.

Table 1. Two-Way ANOVA Results of the Frictional Energy for the Two Different Sliding Speeds and Loads, Respectively^a

	Experimental	6 mN	60 mN	1 mm/s	10 mm/s
No.	Methods	1 vs. 10 mm/s	1 vs. 10 mm/s	6 vs. 60 mN	6 vs. 60 mN
1	$\phi = 1$	ns	ns	****	****
2	$\phi = 0.8, \ a = 3, \ b = 3$	ns	****	****	****
3	$\phi = 0.8, \ a = 6, \ b = 6$	ns	****	****	****
4	$\phi = 0.8, a = 12, b = 12$	ns	****	****	****
5	$\phi = 0.5, \ a = 3, \ b = 12$	ns	****	****	****

ans: not significant; *: p < 0.05; **: p < 0.001; ***: p < 0.0005; ****: p < 0.0001.

significantly increased the COF values at 1 mm/s (p < 0.001) or made no significant difference in the COF values at 10 mm/ s, compared to the smooth surface. On the other hand, at 60 mN, the micropore texturing reduced the COF significantly (p < 0.0001) compared to the smooth surface at both the sliding speeds of 1 and 10 mm/s, except for the case of the micopored surface with the largest pore and gap sizes ($\phi = 0.8$ with a = b= 12 μ m), which significantly increased the COF at a sliding speed of 1 mm/s. The effect of the variations of the pore dimensions among the micopored surfaces also appeared significant for all the cases under 60 mN, showing that the smaller pore dimensions generally helped reduce the COF more effectively. Dunn et al.²⁹ reported that the liquid film thickness formed by tears (viscosity of 1.5 mPa·s) should be at least 2 µm to achieve hydrodynamic lubrication between a smooth contact lens and an eyelid (both with roughness on a nanoscale) at a sliding speed of 10 mm/s during blinking under a contact pressure of a few kPa. According to Yan, 45 the minimum liquid film thickness required for hydrodynamic lubrication between the micropore textures of the pHEMA and a smooth glass curve should be at least in the order of 10 μ m, which is not probable in our test condition having a relatively low aqueous viscosity (1 mPa·s) and slow sliding speed (1-10 mm/s) but a relatively large contact pressure (>10 kPa) and microscale surface roughness of the pore textures. This suggests that the lubrication regime should belong to either a boundary or mixed lubrication regime. Although the increase in the sliding speed generally lowered the COF values, the

order of magnitude difference during the decrease is not more than 1, which also excludes the possibility of the hydrodynamic lubrication regime where a steady liquid film formed at the sliding interface typically causes the decrease in the COF value by several orders of magnitude. $^{46-48}$

Despite the significant differences represented by the COF data for the effects of the load, sliding speed, and micropore texturing on the tribological properties of the pHEMA hydrogel, it should be noted that the COF values under 6 mN show very large standard deviations (as large as ~50 times to the corresponding mean COF values) compared to those under 60 mN (less than the corresponding mean COF values). Such large fluctuations of the standard deviation, especially under a low load of 6 mN, were due to the stick-slip phenomena observed during the tribological experiments (see Supporting Information for the raw data, especially Figure S4 for smooth untextured pHEMA and Figure S5 for micopored pHEMA). Under 6 mN, the COF values of both the smooth and micopored pHEMA surfaces oscillated from near 0 (slipping phase) to over 100 (sticking phase) either along or against the sliding direction. This indicates an unsteady contact mode altered by the kinetic and static friction forces back and forth. The irregular stick-slip friction forces cause the large variations of the COF value. 49 While the stick-slip is a common phenomenon observed during the tribology of soft materials like hydrogels, 50-52 the details behind the stick-slip (related to the self-excited vibration) are complicated and difficult to predict. 53-55 The mean COF values with large

Table 2. Two-Way ANOVA Results of the Frictional Energy of Two Different Surfaces under the Same Load and Speed

				6 mN		60 mN	
No.	Surface A	vs.	Surface B	1 mm/s	10 mm/s	1 mm/s	10 mm/s
(Unter	xtured vs. textured surfaces)						
1	$oldsymbol{\phi}=1$	vs.	$\phi = 0.8, a = 3, b = 3$	ns	ns	****	****
2	$oldsymbol{\phi}=1$	VS.	$\phi = 0.8, a = 6, b = 6$	ns	ns	****	****
3	$\phi = 1$	vs.	$\phi = 0.8, a = 12, b = 12$	ns	ns	ns	****
4	$\phi = 1$	vs.	$\phi = 0.5, a = 3, b = 12$	ns	ns	****	****
(Fixed	(ϕ)						
5	$\phi = 0.8, a = 3, b = 3$	vs.	$\phi = 0.8, a = 6, b = 6$	ns	ns	****	**
6	$\phi = 0.8, a = 3, b = 3$	vs.	$\phi = 0.8, a = 12, b = 12$	ns	ns	****	*
7	$\phi = 0.8, a = 6, b = 6$	VS.	$\phi = 0.8, a = 12, b = 12$	ns	ns	****	ns
(Fixed a)							
8	$\phi = 0.8, a = 3, b = 3$	vs.	$\phi = 0.5, a = 3, b = 12$	ns	ns	****	ns
(Fixed	l b)						1
9	$\phi = 0.8, \ a = 12, \ b = 12$	vs.	$\phi = 0.5, a = 3, b = 12$	ns	ns	****	ns

ans: not significant; *: p < 0.05; **: p < 0.001; ***: p < 0.0005; ****: p < 0.0001.

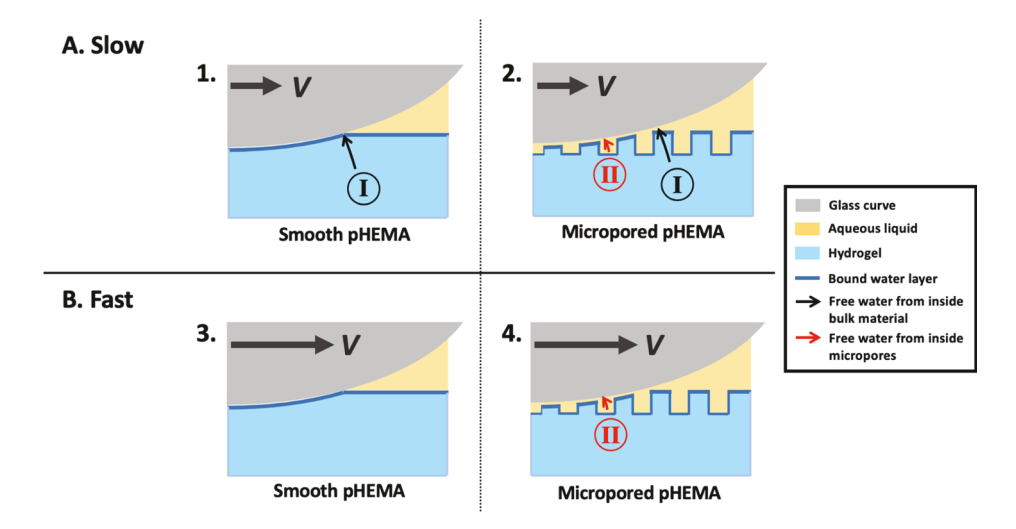


Figure 5. Schematic diagrams (not to scale) of the contact time-dependent movement of free water inside bulk pHEMA (arrow marked as "I") and inside micropores (arrow marked as "II"), respectively. The sliding speeds applied in this study (i.e., both 1 and 10 mm/s) correspond to the case marked as "Fast" (B), where the resident time of the glass curve on the pHEMA surface is less than 5 s. In contrast, "Slow" (A) represents the case that the resident time is greater than 5 s, which is not considered in this study.

fluctuations caused by irregular stick—slip are not suitable to precisely illustrate the effects of the dynamic conditions and the surface morphology on the tribological properties. Therefore, a frictional energy per sliding cycle, which can encompass the different dynamic behaviors (i.e., unsteady or steady state) over the time durations, 32–34 was further calculated and used to interpret the difference among the surfaces, as follows.

3.2. Frictional Energy. Figure 4 exhibits the dissipated frictional energy per sliding cycle (distance of 2×10 mm) of the smooth ($\phi = 1$) and micopored pHEMA surfaces under 6 and 60 mN with sliding speeds of 1 and 10 mm/s. Tables 1 and 2 show the results of the two-way ANOVA analysis, summarizing the significant differences resulting from the exclusive effects of the dynamic conditions (loads and sliding

speeds) at the given micropore texture and the micropore textures at the given dynamic conditions, respectively. While generally agreeing with the COF data (Figure 3) qualitatively, the frictional energy data (Figure 4) show moderate deviations with clearer significance in the differences by the effects of load, sliding speed, and micropore textures. The increase in the sliding speed (from 1 to 10 mm/s) significantly (p < 0.0001) decreased the frictional energy dissipation under 60 mN for the micopored surfaces, regardless of the pore dimensions and solid fractions, while no significant difference was measured for the smooth surface (see Table 1). However, the increase in the sliding speed did not show any significant difference under the lower load (6 mN), regardless of the surface textures. The result also shows that the dissipated frictional energy was significantly lower (p < 0.0001) at the higher load (60 mN)

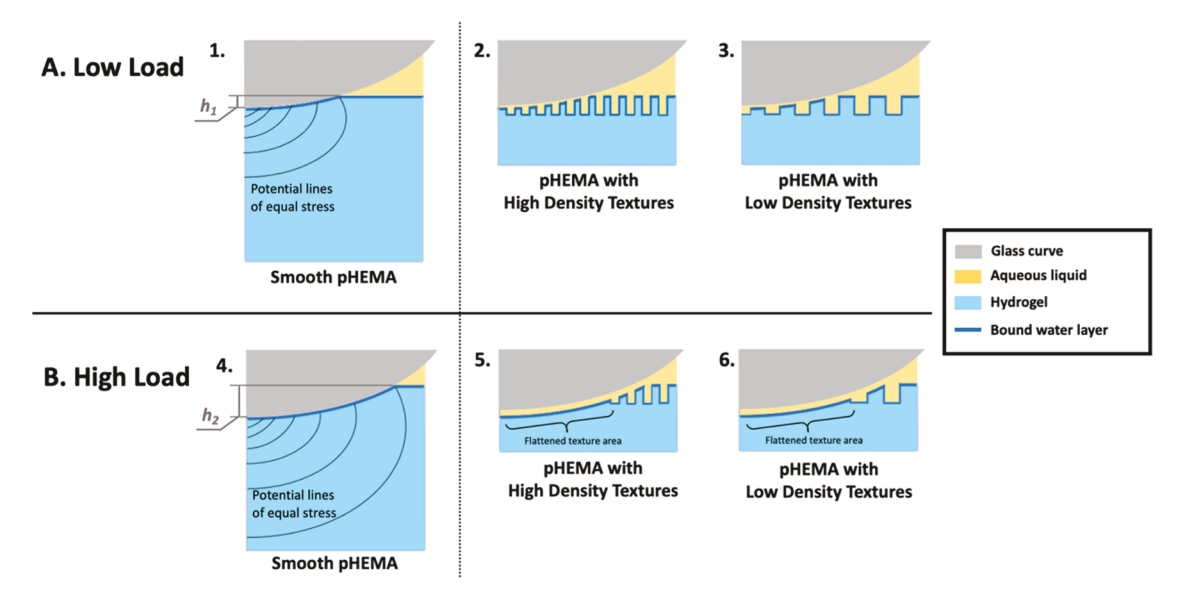


Figure 6. Schematic diagrams of the compression of the pHEMA films with varying loads, where h_1 and h_2 represent the indentation depth under the (A) low load and (B) high load, respectively ($h_1 < h_2$). The thickness of the aqueous film between the glass curve and micopored pHEMA under a low load (2 and 3) is thinner than that under a higher load (5 and 6).

than at the lower load (6 mN), regardless of the sliding speeds and surface textures (see Table 1). Under 6 mN, the surface textures did not show any significant difference in the frictional energy, regardless of the sliding speed (see Table 2). However, under 60 mN, the surface textures showed a significant difference in the frictional energy, which depends on the sliding speed and the pore morphology including the solid fraction and pore dimension (i.e., number density). At a sliding speed of 1 mm/s, the variations of the solid fraction and pore dimension showed a significant difference (p < 0.0001) in every case except for the case of the pored surface of $\phi = 0.8$ with $a = b = 12 \mu m$ in comparison with the smooth surface (ϕ = 1). At a sliding speed of 10 mm/s, all the micopored surfaces showed a significantly lower friction energy (p < 0.0001) than the smooth surface. However, the difference by the variations of the solid fraction and pore dimension among the micopored surfaces was not remarkable but only significant for limited cases of $\phi = 0.8$ with $a = b = 3 \mu \text{m}$ versus $\phi = 0.8$ with a = b =6 μ m (p < 0.001) and ϕ = 0.8 with $a = b = 3 \mu$ m versus ϕ = 0.8 with $a = b = 12 \mu m \ (p < 0.05)$.

The effect of load, sliding speed, and micropore texture of the hydrogel material on the dissipated frictional energy can be understood in association with the availability of the lubricating water layer at the interface, as also suggested by others. 56 According to the wetting theory, 17 the microtextures make a hydrophilic surface more hydrophilic (or superhydrophilic), making the microtextures filled with an aqueous liquid. As a hydrophilic hydrogel, a water droplet shows complete wetting (i.e., a contact angle of $\sim 0^{\circ}$) on a pHEMA surface even without microtextures. The wetting was more pronounced with the micropore textures, making a water droplet spread out more quickly over the pHEMA surface showing the complete wetting almost immediately, agreeing with the wetting theory. 17 As illustrated in Figure 5, the micropores of the hydrophilic hydrogel material of pHEMA can help entrain water into the sliding interface due to the free water occupied within the micropores and hence reduce the dissipated frictional energy at the interface. Besides free water filled into the micropores, the absorbed water inside bulk

pHEMA (~40% water content by weight) can also contribute to lubricate the interface. Less than half (\sim 17%) of the absorbed water in the bulk pHEMA is free (unbound), which is mobile and can readily depart from the polymer under external stimuli such as pressure, while the rest is bound to the polymer and ineffective to contribute to lubricate the interface.⁵⁷ In addition, it takes time for the free water inside the bulk pHEMA to come out to the interface. The Maxwell-Wiechert characterization of the viscoelastic properties of pHEMA (~40% water content) shows that the relaxation time constant τ_1 for the fastest Maxwell element is larger than 5 s. 9,58 This suggests that free water absorbed inside bulk pHEMA should take at least a few seconds to be driven out to the interface. However, in this study, the maximum resident time of the glass curve possible on the pHEMA surface, which is the case when a highest load of 60 mN (resulting in a maximum contact length of 1.90 mm in terms of the diameter of the interfacial contact area) is applied with a slowest sliding speed of 1 mm/s, is less than 2 s. This indicates that there should not be enough time for the free water adsorbed in bulk pHEMA to become available at the interface even at our slowest speed. This is schematically explained in Figure 5B as "Fast" (i.e., both speeds of 1 and 10 mm/s can be regarded as fast), where the resident time of the glass curve on the pHEMA surface is less than 5 s so that the interfacial lubrication by the free water is mainly effective for the case of micopored surfaces but not for the smooth surface. Although the pHEMA hydrogel is, strictly speaking, a viscoelastic material due to its water content, the research^{9,58} also suggests that the elastic properties of pHEMA (with ~1% EDGMA crosslinkers) play a dominant role during the material relaxation process when the compression duration is less than 5 s. Therefore, the Hertzian contact theory applied to this study is suitable for pHEMA showing the contact durations between the glass curve and the pHEMA surface less than 2 s.

Meanwhile, Table 1 shows that the increase in the sliding speed from 1 to 10 mm/s under the domain of fast sliding (Figure 5B) significantly decreases the frictional energy only for the case of the relatively high load (60 mN) for the

micopored surfaces. This is attributed to the significantly greater amount of free water from the micropores with an increase in the load, as illustrated in Figure 6, increasing the continuity of the aqueous lubricating film at the interface. Under 60 mN, the indentation depth of the glass curve (\sim 30 um as calculated using the Hertzian contact theory; see Table S3 in Supporting Information) is much greater than the depth of a micropore (12 μ m). As illustrated in Figure 6B, this makes the micopored surface almost flattened (it is estimated that ~60% of the textures under the interfacial contact area would be flattened under 60 mN with an indentation depth of ~30 μ m) so that most of the free water occupied inside the micropores will become entrained at the interface and enhance the lubricating effect more significantly with a higher level of the continuity of the interfacial aqueous film on the micopored pHEMA surface. This makes the lubrication regime closer toward a hydrodynamic lubrication, as suggested by the decrease in the order of magnitude of the COF value from 1 to 0.3 along with an increase in the sliding speed from 1 to 10 mm/s under 60 mN. The effect of the load on the frictional energy appears more evidently at the given sliding speed and surface texture, as also shown in Table 1. The result suggests that the tribological behaviors of the soft hydrogel material would not follow the conventional Stribeck curve, where the increase in the load makes the lubrication regime favorable toward boundary lubrication, while the increase in the sliding speed makes the lubrication regime favorable toward hydrodynamic lubrication. In this study, the pHEMA hydrogel shows that the increase in the load can make the lubrication regime favorable toward hydrodynamic lubrication due to the increase in the amount of the lubricating aqueous liquid at the interface, which can further be enhanced by the micropore textures, while the general trend by the increase in the sliding speed is not altered.

Under a relatively low load of 6 mN, the maximum indentation depth at the center calculated using the Hertzian contact theory (see Table S3 in Supporting Information) is not more than \sim 6 μ m, which is around a half of the depth of a micropore. As illustrated in Figure 6A, despite the compression, the micropore textures under a relatively low load can maintain the pored nature with a much smaller interfacial contact area with the sliding glass curve than under the high load. For example, the interfacial contact area under 6 mN ($\sim \pi \times (439 \pm 12 \,\mu\text{m})^2$) is about a quarter of the contact area under 60 mN ($\sim \pi \times (946 \pm 26 \ \mu \text{m})^2$). Due to the reduced compression under lower load, a significantly less amount of free water is released to form the lubricating layer at the interface. Therefore, even with an increase in the sliding speed, pore-texturing was not effective in significantly reducing the frictional energy under a relatively low load. The variations of the solid fraction and pore dimension were not effective either to reduce the friction energy under a relatively low load of 6 mN, as shown in Table 2.

Under a relatively high load of 60 mN, the pore textures of the varying solid fractions and pore dimensions were all effective to significantly reduce the frictional energy compared to the smooth (untextured) surface within the relatively fast sliding regime (1–10 mm/s), as also summarized in Table 2. Only exception was for the case of the pored surface of $\phi = 0.8$ with a = b = 12 at 1 mm/s. The dimensions of the pore diameter (b) and the gap size (a) are the largest ones among the pore textures tested in this study, leading to the lowest number density of the pore pattern per given surface area. It is

expected that a finer pore with a higher number density (i.e., small pore diameter and gap size) will reduce the friction force more effectively since the lubricant liquid can be retained within the smaller pore more robustly against external forces and the lubricant liquid exposed at the top solid surface can be maintained more stably when the gap size is smaller. 59,60 At a given solid area fraction of $\phi = 0.8$, the pored surface with a smaller pore dimension indeed shows a more significant reduction in the frictional energy at a sliding speed of 1 mm/s (Figure 4). The reduction decreases as the pore dimensions increase; for the pored surface of the largest dimensions (a = b= 12), there is no significant reduction compared to the smooth (untextured) surface. This is attributed to the relatively large pore dimensions that result in the relatively low amount and continuity of the aqueous lubricious film at the interface. Such geometric effects can also be confirmed when comparing the pored surfaces of the same gap size but different pore diameters (i.e., $\phi = 0.8$ with a = 3 and b = 3 versus $\phi = 0.5$ with a = 3 and b = 12) or those of the same pore size but different gap sizes (i.e., $\phi = 0.8$ with a = 12 and b = 12 versus ϕ = 0.5 with a = 3 and b = 12). They show that the increase in the pore size (b) at the same gap size or the increase in the gap size (a) at the same pore size results in the increase in the frictional energy (Figure 4), as expected. However, the effect of the texture feature size on friction, which is also strongly dependent on the other parameters of the tribological system, cannot be generalized in a predictable manner. 61 For example, the pored surface of $\phi = 0.8$ with a = b = 12 shows significant reduction in the frictional energy compared to the smooth (untextured) surface at an increased sliding speed of 10 mm/s. Also, the variations of the solid area fractions and pore dimensions among the pored surfaces at a higher sliding speed of 10 mm/s do not show a remarkable difference in the frictional energy.

Our results fundamentally agree with the other reports where pored hydrogel surfaces had been found to improve the lubrication at the interface. 62,63 While the pore patterns employed in this study for the pHEMA hydrogel are ordered and uniform over the surface, it had also been found that random micropore structures of polyvinyl alcohol hydrogels could also help maintain a large amount of water at the interface to increase the continuity of the lubricate aqueous film.⁵⁶ Such a lubrication mechanism had also been found within articular cartilage, which contains a large amount of water within the pored network on the surfaces.⁶⁴ Of note, it had also been reported that the friction was more affected by the lubrication condition and applied load rather than the hydrogel polymer concentration and polymerization.⁵⁶ Our result also shows that the friction of the micropore-textured hydrogel surface is highly dependent on the load and the interfacial lubrication condition.

3.3. Effects of Hydrophilicity. Our previous study showed that micopored PDMS with a solid area fraction of 0.8–0.9 and a pore diameter of 5 μ m (similar textures tested in this study for pHEMA) increased the friction force in most cases under the boundary and mixed lubrication regimes, as opposed to this study showing the significant reduction in the friction force by the micropore textures. It is attributed to the different surface wettabilities between PDMS and pHEMA. While PDMS is a hydrophobic material, pHEMA is a hydrophilic hydrogel. While air-trapping commonly occurs within the pores under a hydrophobic condition, ^{65,66} the pores under a hydrophilic condition are typically completely wetted

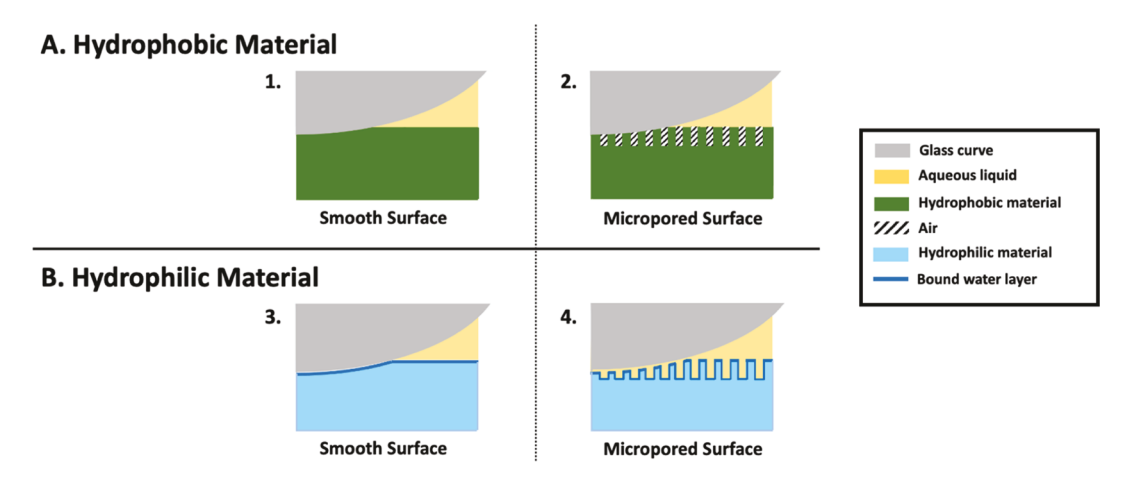


Figure 7. Schematic diagrams of the interfaces formed on (A) hydrophobic polymer (e.g., PDMS) and (B) hydrophilic hydrogel (e.g., pHEMA), respectively, under the load in the aqueous liquid environment.

by the aqueous liquid, ^{17,67,68} as illustrated in Figure 7. The hydrophobicity of PDMS causes the air-trapping in the micropores, preventing water from entering the pore textures; this creates the instability of the liquid film with discontinuity at the interface and eventually reduces the lubricating effect of the interfacial liquid film. However, the hydrophilicity of pHEMA ensures the complete wetting of the aqueous liquid to the pores and the formation of an efficient aqueous lubrication layer with little discontinuity at the interface. In addition, the micropores help retain the water within them due to wall friction, which can further be enhanced by the possible nanoscale dangling polymer chains on the surface. ^{37,38,68} Our results show that the hydrophilicity of the substrate polymer material is important in employing micropore textures to reduce tribological friction in a physiologically relevant aqueous environment.

Although PDMS can be treated to be hydrophilic,⁶⁸ the hydrophilicity usually degrades over time^{69,70} so that the PDMS material is generally not suitable for a long-term implant application as a hydrophilic material. Compared to PDMS, pHEMA has much lower stiffness (~10⁵ softer in terms of Young's modulus), requiring much less energy (or force) to achieve the same deformation or bringing out more water retained inside pores to the contact interface with a larger deformation under the same load, especially when the indentation depth is less than the pore depth. Moreover, the most significant uniqueness of pHEMA is the nature of the hydrogel material and its effect on the availability of water at the interface. There should always be an "available path" for free water to move from the hydrogel material or the surrounding aqueous area to the contact interface.

Of note, in this study, we used frictional energy to compare the tribological properties of the textured hydrogel material to those of the untextured one, whereas we had used the COF values in our previous study of PDMS.² This is because the standard deviations in the measured COF data were relatively smaller in the case of PDMS, which was not the case for the pHEMA hydrogel. It should also be noted that there were much less stick—slip phenomena in the study of PDMS than that of pHEMA, leading to a steadier tribological system. Hence, the COF values were suitable enough for the PDMS study. Although the COF values generally showed a similar trend to the frictional energy affected by the dynamic conditions (load and sliding speed) and micropore textures

in this study of the pHEMA hydrogel, the frictional energy is a better way to represent the tribological properties of the hydrogel material with complex and unsteady dynamic behaviors.

4. CONCLUSIONS

Micropore textures significantly affected the tribological properties of pHEMA hydrogel surfaces, which depended on the loads and sliding speeds applied as well as the pore dimensions. Overall, due to the ability to store a large amount of free water within their textures, the micopored pHEMA surfaces have the potential to reduce friction, leading to less wear of the surfaces. Our study reveals that micropore texturing to the pHEMA hydrogel significantly decreased the COF and frictional energy at a relatively high load with a relatively fast sliding speed. Although a slight increase in the friction can occur at a low load with a relatively slow sliding speed, which also depends on the pore size and density, the friction can generally be decreased by employing the micropore texturing to the hydrogel when the sliding speed is relatively fast, which is still within the physiologically relevant level. This opposes the results shown with the hydrophobic polymer material such as PDMS, suggesting that the hydrophilicity of the hydrogel material makes a significant difference in the tribological properties. Our results suggest that the pHEMA hydrogels with carefully designed micropore textures can benefit biomedical applications such as implant and ophthalmology by reducing the interfacial friction in the aqueous environment and hence lowering the chance of inflammation, such as near a contact lens or keratoprosthesis.

ASSOCIATED CONTENT

Supporting Information

The Supporting Information is available free of charge at https://pubs.acs.org/doi/10.1021/acsami.1c13718.

Estimation of the contact pressure; indentation depth and effect of loads on the material's Young's modulus; real-time sliding velocity plots; roughness of a glass curve; results of t-test analysis of the COF mean values; and time-dependent raw data of normal force (F_z) , friction force (F_x) , and COF values (PDF)

AUTHOR INFORMATION

Corresponding Authors

Prashant Kumar Sharma — Department of Biomedical Engineering (FB40), University of Groningen and University Medical Center Groningen, Groningen 9713AV, The Netherlands; Email: p.k.sharma@umcg.nl

Chang-Hwan Choi — Department of Mechanical Engineering, Stevens Institute of Technology, Hoboken, New Jersey 07030, United States; o orcid.org/0000-0003-2715-7393; Email: cchoi@stevens.edu

Authors

Yiwen Xi — Department of Mechanical Engineering, Stevens Institute of Technology, Hoboken, New Jersey 07030, United States; Department of Biomedical Engineering (FB40), University of Groningen and University Medical Center Groningen, Groningen 9713AV, The Netherlands

Hans Jan Kaper – Department of Biomedical Engineering (FB40), University of Groningen and University Medical Center Groningen, Groningen 9713AV, The Netherlands

Complete contact information is available at: https://pubs.acs.org/10.1021/acsami.1c13718

Author Contributions

The manuscript was written through contributions of all authors. All authors have given approval to the final version of the manuscript. Y.X. and C.-H.C. designed and fabricated the microtextured samples. Y.X., H.J.K., and P.K.S. designed and carried out the tribological experiments. All authors contributed to the analysis of the data.

Notes

The authors declare no competing financial interest.

ACKNOWLEDGMENTS

We gratefully acknowledge the Graduate School of Medical Sciences, UMCG, for the scholarship to Y.X. for the collaborative Ph.D. program. The grant no. 91112026 from the Netherlands Organization for Health Research and Development (ZonMW) is duly acknowledged for the purchase of the UMT-3 device. We also gratefully acknowledge the Stevens Institute of Technology for the Innovation and Entrepreneurship (I&E) Doctoral Fellowship, the Excellence Doctoral Fellowship, and the grant from the SPRINT program to Y.X. We also recognize the funding support from the National Science Foundation (NSF) with the Innovation Corps (I-Corps) program (award number 1946450).

■ REFERENCES

- (1) Li, L.; Zhong, Y.; Gong, J.; Li, J.; Huang, J.; Ma, Z. Fabrication of Robust Micro-Patterned Polymeric Films via Static Breath-Figure Process and Vulcanization. *J. Colloid Interface Sci.* **2011**, 354, 758–764.
- (2) Xi, Y.; Kaper, H. J.; Choi, C.-H.; Sharma, P. K. Tribological Properties of Microporous Polydimethylsiloxane (PDMS) Surfaces under Physiological Conditions. *J. Colloid Interface Sci.* **2020**, *561*, 220–230
- (3) Wang, Y.; Subbiahdoss, G.; Swartjes, J.; van der Mei, H. C.; Busscher, H. J.; Libera, M. Length-Scale Mediated Differential Adhesion of Mammalian Cells and Microbes. *Adv. Funct. Mater.* **2011**, 21, 3916–3923.
- (4) Alves, N. M.; Pashkuleva, I.; Reis, R. L.; Mano, J. F. Controlling Cell Behavior through the Design of Polymer Surfaces. *Small* **2010**, *6*, 2208–2220.

- (5) Moroni, L.; Licht, R.; de Boer, J.; de Wijn, J. R.; van Blitterswijk, C. A. Fiber Diameter and Texture of Electrospun PEOT/PBT Scaffolds Influence Human Mesenchymal Stem Cell Proliferation and Morphology, and the Release of Incorporated Compounds. *Biomaterials* **2006**, 27, 4911–4922.
- (6) Mata, A.; Kim, E. J.; Boehm, C. A.; Fleischman, A. J.; Muschler, G. F.; Roy, S. Three-Dimensional Scaffold with Precise Micro-Architecture and Surface Micro-Textures. *Biomaterials* **2009**, *30*, 4610–4617.
- (7) Nguyen, Q. T.; Hwang, Y.; Chen, A. C.; Varghese, S.; Sah, R. L. Cartilage-like Mechanical Properties of Poly (ethylene glycol)-Diacrylate Hydrogels. *Biomaterials* **2012**, *33*, 6682–6690.
- (8) Parlato, M.; Reichert, S.; Barney, N.; Murphy, W. L. Poly(ethylene glycol) Hydrogels with Adaptable Mechanical and Degradation Properties for Use in Biomedical Applications. *Macromol. Biosci.* **2014**, *14*, 687–698.
- (9) Kaufman, J. D.; Miller, G. J.; Morgan, E. F.; Klapperich, C. M. Time-Dependent Mechanical Characterization of Poly (2-hydroxyethyl methacrylate) Hydrogels Using Nanoindentation and Unconfined Compression. *J. Mater. Res.* **2008**, 23, 1472–1481.
- (10) Wang, Z.; Volinsky, A. A.; Gallant, N. D. Crosslinking Effect on Polydimethylsiloxane Elastic Modulus Measured by Custom-Built Compression Instrument. *J. Appl. Polym. Sci.* **2014**, *131*, 41050.
- (11) Patel, P. S.; Shepherd, D. E.; Hukins, D. W. Compressive Properties of Commercially Available Polyurethane Foams as Mechanical Models for Osteoporotic Human Cancellous Bone. *BMC Muscoskel. Disord.* **2008**, *9*, 137.
- (12) Ahmed, E. M. Hydrogel: Preparation, Characterization, and Applications: A Review. J. Adv. Res. 2015, 6, 105–121.
- (13) Akhtar, M. F.; Hanif, M.; Ranjha, N. M. Methods of synthesis of hydrogels ... A review. *Saudi Pharmaceut. J.* **2016**, 24, 554–559.
- (14) Caló, E.; Khutoryanskiy, V. V. Biomedical Applications of Hydrogels: A Review of Patents and Commercial Products. *Eur. Polym. J.* **2015**, *65*, 252–267.
- (15) Pfister, P. M.; Wendlandt, M.; Neuenschwander, P.; Suter, U. W. Surface-Textured PEG-Based Hydrogels with Adjustable Elasticity: Synthesis and Characterization. *Biomaterials* **2007**, *28*, 567–575.
- (16) Choi, Y. S.; Vincent, L. G.; Lee, A. R.; Kretchmer, K. C.; Chirasatitsin, S.; Dobke, M. K.; Engler, A. J. The Alignment and Fusion Assembly of Adipose-Derived Stem Cells on Mechanically Patterned Matrices. *Biomaterials* **2012**, *33*, 6943–6951.
- (17) Bico, J.; Thiele, U.; Quéré, D. Wetting of Textured Surfaces. *Colloids Surf., A* **2002**, 206, 41–46.
- (18) Etsion, I. Improving Tribological Performance of Mechanical Components by Laser Surface Texturing. *Tribol. Lett.* **2004**, *17*, 733–737
- (19) Etsion, I. State of the Art in Laser Surface Texturing. J. Tribol. 2005, 127, 248–253.
- (20) Kovalchenko, A.; Ajayi, O.; Erdemir, A.; Fenske, G.; Etsion, I. The Effect of Laser Surface Texturing on Transitions in Lubrication Regimes during Unidirectional Sliding Contact. *Tribol. Int.* **2005**, 38, 210, 225
- (21) Shinkarenko, A.; Kligerman, Y.; Etsion, I. The Effect of Surface Texturing in Soft Elasto-Hydrodynamic Lubrication. *Tribol. Int.* **2009**, 42, 284–292.
- (22) Chirani, N.; Yahia, L. H.; Gritsch, L.; Motta, F. L.; Chirani, S.; Farè, S. History and Applications of Hydrogels. *J. Biomed. Sci.* **2015**, *4*, 13.
- (23) McMahon, T. T.; Zadnik, K. Twenty-Five Years of Contact Lenses: The Impact on the Cornea and Ophthalmic Practice. *Cornea* **2000**, *19*, 730–740.
- (24) Chirila, T. V. An Overview of the Development of Artificial Corneas with Porous Skirts and the Use of pHEMA for Such an Application. *Biomaterials* **2001**, *22*, 3311–3317.
- (25) Sterner, O.; Karageorgaki, C.; Zürcher, M.; Zürcher, S.; Scales, C. W.; Fadli, Z.; Spencer, N. D.; Tosatti, S. G. P. Reducing Friction in the Eye: A Comparative Study of Lubrication by Surface-Anchored Synthetic and Natural Ocular Mucin Analogues. ACS Appl. Mater. Interfaces 2017, 9, 20150–20160.

- (26) Meakin, J. R.; Hukins, D. W. L.; Aspden, R. M.; Imrie, C. T. Rheological Properties of Poly (2-hydroxyethyl methacrylate) (pHEMA) As a Function of Water Content and Deformation Frequency. J. Mater. Sci.: Mater. Med. 2003, 14, 783–787.
- (27) Choi, S. H.; Park, K. S.; Sung, M.-W.; Kim, K. H. Dynamic and Quantitative Evaluation of Eyelid Motion Using Image Analysis. *Med. Biol. Eng. Comput.* **2003**, *41*, 146–150.
- (28) Choi, S.-H.; Yoon, T. H.; Lee, K.-S.; Ahn, J. H.; Chung, J. W. Blepharokymographic Analysis of Eyelid Motion in Bell's Palsy. *Laryngoscope* **2007**, *117*, 308–312.
- (29) Dunn, A. C.; Tichy, J. A.; Urueña, J. M.; Sawyer, W. G. Lubrication Regimes in Contact Lens Wear during a Blink. *Tribol. Int.* **2013**, *63*, 45–50.
- (30) Rennie, A. C.; Dickrell, P. L.; Sawyer, W. G. Friction Coefficient of Soft Contact Lenses: Measurements and Modeling. *Tribol. Lett.* **2005**, *18*, 499–504.
- (31) Collaborative Normal-Tension Glaucoma Study Group. Comparison of Glaucomatous Progression between Untreated Patients with Normal-Tension Glaucoma and Patients with Therapeutically Reduced Intraocular Pressures. *Am. J. Ophthalmol.* **1998**, 126, 487–497.
- (32) Ramalho, A.; Miranda, J. C. The Relationship between Wear and Dissipated Energy in Sliding Systems. Wear 2006, 260, 361–367.
- (33) Bryant, M. D.; Khonsari, M. M.; Ling, F. F. On the Thermodynamics of Degradation. *Proc. R. Soc. A* **2008**, 464, 2001–2014
- (34) Aghdam, A. B.; Khonsari, M. M. Prediction of Wear in Reciprocating Dry Sliding via Dissipated Energy and Temperature Rise. *Tribol. Lett.* **2013**, *50*, 365–378.
- (35) Pitenis, A. A.; Manuel Urueña, J.; Nixon, R. M.; Bhattacharjee, T.; Krick, B. A.; Dunn, A. C.; Angelini, T. E.; Gregory Sawyer, W. Lubricity from Entangled Polymer Networks on Hydrogels. *J. Tribol.* **2016**, *138*, 042102.
- (36) Peppas, N. A.; Moynihan, H. J.; Lucht, L. M. The Structure of Highly Crosslinked Poly (2-hydroxyethyl methacrylate) Hydrogels. *J. Biomed. Mater. Res.* **1985**, *19*, 397–411.
- (37) Zhang, X.; Xu, J.; Okawa, K.; Katsuyama, Y.; Gong, J.; Osada, Y.; Chen, K. In Situ Monitoring of Hydrogel Polymerization Using Speckle Interferometry. *J. Phys. Chem. B* **1999**, *103*, 2888–2891.
- (38) Meier, Y. A.; Zhang, K.; Spencer, N. D.; Simic, R. Linking Friction and Surface Properties of Hydrogels Molded against Materials of Different Surface Energies. *Langmuir* **2019**, *35*, 15805–15812.
- (39) Kim, S. H.; Opdahl, A.; Marmo, C.; Somorjai, G. A. AFM and SFG Studies of pHEMA-Based Hydrogel Contact Lens Surfaces in Saline Solution: Adhesion, Friction, and the Presence of Noncrosslinked Polymer Chains at the Surface. *Biomaterials* **2002**, 23, 1657–1666.
- (40) Tsukruk, V. V.; Huang, Z.; Chizhik, S. A.; Gorbunov, V. V. Probing of Micromechanical Properties of Compliant Polymeric Materials. *J. Mater. Sci.* **1998**, 33, 4905–4909.
- (41) Park, S.; Costa, K. D.; Ateshian, G. A. Microscale Frictional Response of Bovine Articular Cartilage from Atomic Force Microscopy. *J. Biomech.* **2004**, *37*, 1679–1687.
- (42) Shoaib, T.; Espinosa-Marzal, R. M. Insight into the Viscous and Adhesive Contributions to Hydrogel Friction. *Tribol. Lett.* **2018**, *66*, 96.
- (43) Gong, J.-P.; Onaivi, E. S.; Ishiguro, H.; Liu, Q.-R.; Tagliaferro, P. A.; Brusco, A.; Uhl, G. R. Cannabinoid CB2 Receptors: Immunohistochemical Localization in Rat Brain. *Brain Res.* **2006**, *1071*, 10–23.
- (44) Kurokawa, T.; Uji, S.; Suzuki, T. Identification of cDNA Coding for a Homologue to Mammalian Leptin from Pufferfish, Takifugu Rubripes. *Peptides* **2005**, *26*, 745–750.
- (45) Yan, Y. Tribology and tribo-corrosion testing and analysis of metallic biomaterials. *Metals for Biomedical Devices*; Woodhead Publishing, 2010, pp 178–201.
- (46) Eder, S. J.; Ielchici, C.; Krenn, S.; Brandtner, D. An Experimental Framework for Determining Wear in Porous Journal

- Bearings Operated in the Mixed Lubrication Regime. *Tribol. Int.* **2018**, *123*, 1–9.
- (47) Hamrock, B. J.; Schmid, S. R.; Jacobson, B. O. Fundamentals of Fluid Film Lubrication; CRC Press, 2004; Vol. 114, pp 741–756.
- (48) Hess, D. P.; Soom, A. Friction at a Lubricated Line Contact Operating at Oscillating Sliding Velocities. *J. Tribol.* **1990**, *112*, 147–152.
- (49) Gao, C.; Kuhlmann-Wilsdorf, D. On Stick-Slip and the Velocity Dependence of Friction at Low Speeds. *J. Tribol.* **1990**, *112*, 354–360.
- (50) Jiménez, A.-E.; Bermúdez, M.-D. Friction and wear. *Tribology for Engineers*; Woodhead Publishing, 2011; pp 33-63.
- (51) Shoaib, T.; Nalam, P. C.; He, Y.; Chen, Y.; Espinosa-Marzal, R. M. Assembly, Morphology, Diffusivity, and Indentation of Hydrogel-Supported Lipid Bilayers. *Langmuir* **2017**, 33, 7105–7117.
- (\$2) Bhamra, T. S.; Tighe, B. J. Mechanical Properties of Contact Lenses: The Contribution of Measurement Techniques and Clinical Feedback to 50 Years of Materials Development. *Contact Lens Anterior Eye* **2017**, 40, 70–81.
- (53) Tang, L.; Zhu, X.; Qian, X.; Shi, C. Effects of Weight on Bit on Torsional Stick-Slip Vibration of Oilwell Drill String. *J. Mech. Sci. Technol.* **2017**, *31*, 4589–4597.
- (54) Ranjbar, M.; Nahid, M.; Renawi, A.; Sadeqi, Z. Development of an Educational Noise Reduction Measurement Test Bench. *J. Rob. Mechatron. Syst.* **2017**, *2*, 27–32.
- (55) Earles, S. W. E.; Chambers, P. W. Disc Brake Squeal Noise Generation: Predicting Its Dependency on System Parameters Including Damping. *Int. J. Veh. Des.* 1987, 8, 538–552.
- (56) Shi, Y.; Xiong, D. Microstructure and Friction Properties of PVA/PVP Hydrogels for Articular Cartilage Repair as Function of Polymerization Degree and Polymer Concentration. *Wear* **2013**, *305*, 280–285.
- (57) Tranoudis, I.; Efron, N. Water Properties of Soft Contact Lens Materials. Contact Lens Anterior Eye 2004, 27, 193-208.
- (58) Bush, B. G.; Shapiro, J. M.; DelRio, F. W.; Cook, R. F.; Oyen, M. L. Mechanical Measurements of Heterogeneity and Length Scale Effects in PEG-Based Hydrogels. *Soft Matter* **2015**, *11*, 7191–7200.
- (59) Xie, H.; Mead, J.; Wang, S.; Huang, H. The Effect of Surface Texture on the Kinetic Friction of a Nanowire on a Substrate. *Sci. Rep.* **2017**, *7*, 44907.
- (60) Tong, R.; Quan, Z.; Zhao, Y.; Han, B.; Liu, G. Influence of Nanoscale Textured Surfaces and Subsurface Defects on Friction Behaviors by Molecular Dynamics Simulation. *Nanomaterials* **2019**, *9*, 1617.
- (61) Greiner, C.; Merz, T.; Braun, D.; Codrignani, A.; Magagnato, F. Optimum Dimple Diameter for Friction Reduction with Laser Surface Texturing: The Effect of Velocity Gradient. *Surf. Topogr.: Metrol. Prop.* **2015**, *3*, 044001.
- (62) Caravia, L.; Dowson, D.; Fisher, J.; Corkhill, P. H.; Tighe, B. J. A Comparison of Friction in Hydrogel and Polyurethane Materials for Cushion-Form Joints. *J. Mater. Sci.: Mater. Med.* **1993**, *4*, 515–520.
- (63) Li, F.; Su, Y.; Wang, J.; Wu, G.; Wang, C. Influence of Dynamic Load on Friction Behavior of Human Articular Cartilage, Stainless Steel and Polyvinyl Alcohol Hydrogel as Artificial Cartilage. *J. Mater. Sci.: Mater. Med.* **2010**, *21*, 147–154.
- (64) Ateshian, G. A.; Warden, W. H.; Kim, J. J.; Grelsamer, R. P.; Mow, V. C. Finite Deformation Biphasic Material Properties of Bovine Articular Cartilage from Confined Compression Experiments. *J. Biomech.* **1997**, *30*, 1157–1164.
- (65) Martines, E.; Seunarine, K.; Morgan, H.; Gadegaard, N.; Wilkinson, C. D. W.; Riehle, M. O. Air-Trapping on Biocompatible Nanopatterns. *Langmuir* **2006**, *22*, 11230–11233.
- (66) Madaeni, S. S.; Zinadini, S.; Vatanpour, V. Preparation of Superhydrophobic Nanofiltration Membrane by Embedding Multiwalled Carbon Nanotube and Polydimethylsiloxane in Pores of Microfiltration Membrane. Sep. Purif. Technol. 2013, 111, 98–107.
- (67) Di, Z.; Shi, Z.; Ullah, M. W.; Li, S.; Yang, G. A Transparent Wound Dressing Based on Bacterial Cellulose Whisker and Poly (2-hydroxyethyl methacrylate). *Int. J. Biol. Macromol.* **2017**, *105*, 638–644.

- (68) Huang, W.; Jiang, L.; Zhou, C.; Wang, X. The Lubricant Retaining Effect of Micro-Dimples on the Sliding Surface of PDMS. *Tribol. Int.* **2012**, *52*, 87–93.
- (69) Eddington, D. T.; Puccinelli, J. P.; Beebe, D. J. Thermal Aging and Reduced Hydrophobic Recovery of Polydimethylsiloxane. *Sens. Actuators, B* **2006**, *114*, 170–172.
- (70) Gökaltun, A.; Kang, Y. B.; Yarmush, M. L.; Usta, O. B.; Asatekin, A. Simple Surface Modification of Poly(dimethylsiloxane) via Surface Segregating Smart Polymers for Biomicrofluidics. *Sci. Rep.* **2019**, *9*, 7377.

SUPPORTING INFORMATION

Tribological Properties of Micropored pHEMA Hydrogel in Biomimetic

Aqueous Environment

Yiwen Xi^{1,2}, Prashant Kumar Sharma^{2*}, Hans Jan Kaper², Chang-Hwan Choi^{1*}

¹ Department of Mechanical Engineering, Stevens institute of Technology, Castle Point on Hudson, Hoboken,

New Jersey 07030, United States

²University of Groningen and University Medical Center Groningen, Department of Biomedical Engineering

(FB40), Antonius Deusinglaan 1, 9713AV Groningen, The Netherlands

* Corresponding authors:

Prashant Kumar Sharma: p.k.sharma@umcg.nl

Chang-Hwan Choi: cchoi@stevens.edu

ESTIMATION OF THE CONTACT PRESSURE AND INDENTATION DEPTH

Against the applied normal force by a glass curve, the pHEMA hydrogel should be deformed. The contact pressure and indentation depth by the glass curve was estimated by the Hertzian contact theory. For the given load, the average contact pressure, *P*, over the compressed pHEMA interface by the glass curve was estimated by

$$P = \frac{F}{\pi r_{HC}^2} \tag{1}$$

where F is the normal load, and r_{HC} is the contact radius of a glass curve on the pHEMA film. According to the Hertzian contact theory, r_{HC} was obtained as

$$r_{HC} = \sqrt[3]{\frac{3}{4} \frac{FR}{E^*}} \tag{2}$$

where R is the radius of the glass curve (30 mm). E^* is the interfacial stiffness which can be calculated by

$$\frac{1}{E^*} = \frac{1 - v_1^2}{E_1} + \frac{1 - v_2^2}{E_2} \tag{3}$$

where E_I , E_2 and v_I , v_2 are the Young's moduli and Poisson's ratios for glass (subscript 1) and pHEMA (subscript 2), respectively. The Young's modulus of the pHEMA hydrogel in the wet condition should vary depending on the contact pressure because the amount of the water occupying the hydrogel material changes with the pressure. To account for the effect, the Young's modulus of the untextured smooth pHEMA film was measured for varying pressures, and their averaged value was used as E_2 as approximation. The Young's modulus was measured by the Universal Micro-Tribometer (UMT-3, Bruker, Billerica, MA, USA) with a stainless steel pin with a flat contact surface (no curvature, circular cross section of a radius $r_{flat-steel} = 3$ mm) for varying loads (final contact load, $F_{flat-steel} = 0.25$, 0.5, 1, 3, and 5 N) in the phosphate-buffered saline (PBS, pH = 7.4) solution at 33°C. The Young's modulus of the smooth pHEMA hydrogel (E_{pHEMA}) was computed as

$$E_{pHEMA} = \frac{stress}{strain} = \frac{F_{flat-steel}/A}{\Delta L/L_0} = \frac{P_{flat-steel}}{\Delta L/L_0}$$
(4)

where A is the contact area $(\pi r_{flat-steel}^2 = 28.3 \text{ mm}^2)$, ΔL is the displacement of the smooth pHEMA

hydrogel under the final contact load ($F_{flat-steel}$), L_0 is the initial thickness of the smooth pHEMA film with no load applied (\sim 1 mm), and $P_{flat-steel}$ is the final contact pressure. As for the indentation depth, the maximum depth of the pHEMA film at the center of the glass curve was estimated as

$$H_{HC} = \frac{r_{HC}^2}{R} \tag{5}$$

Table S1 and Figure S1 show the indentation depth (ΔL) and the Young's modulus of the smooth pHEMA hydrogel film (E_{pHEMA}) measured by the UMT-3 at the varying normal loads (i.e., contact pressures). The indentation depth increases from 7 to 73 μm with the increase in the contact pressure from 9 to 177 kPa. The Young's modulus increases from 0.88 to 1.71 MPa with the increase in the contact pressure, giving the averaged Young's modulus value (E_2) of 1.2 ± 0.1 MPa for the given contact pressure range (Table S2). The average contact pressure, radius of contact area, and indentation depth estimated for the tribological experiment conditions based on the Hertzian contact theory is also summarized in Table S3.

Table S1. Indentation depth and Young's modulus of the untextured smooth pHEMA film for the varying load and the corresponding contact pressure.

Final Load, F _{flat-steel} (N)	Contact Pressure, P _{flat-steel} (kPa)	Indentation Depth, <i>H</i> _{flat-steel} (μm)	Young's Modulus, E_{pHEMA} (MPa)
0.25	9	7 ± 0.4	0.88 ± 0.05
0.5	18	13 ± 0.7	0.92 ± 0.05
1	35	23 ± 3.8	1.08 ± 0.17
3	106	54 ± 10.7	1.40 ± 0.27
5	177	73 ± 9.4	1.71 ± 0.23

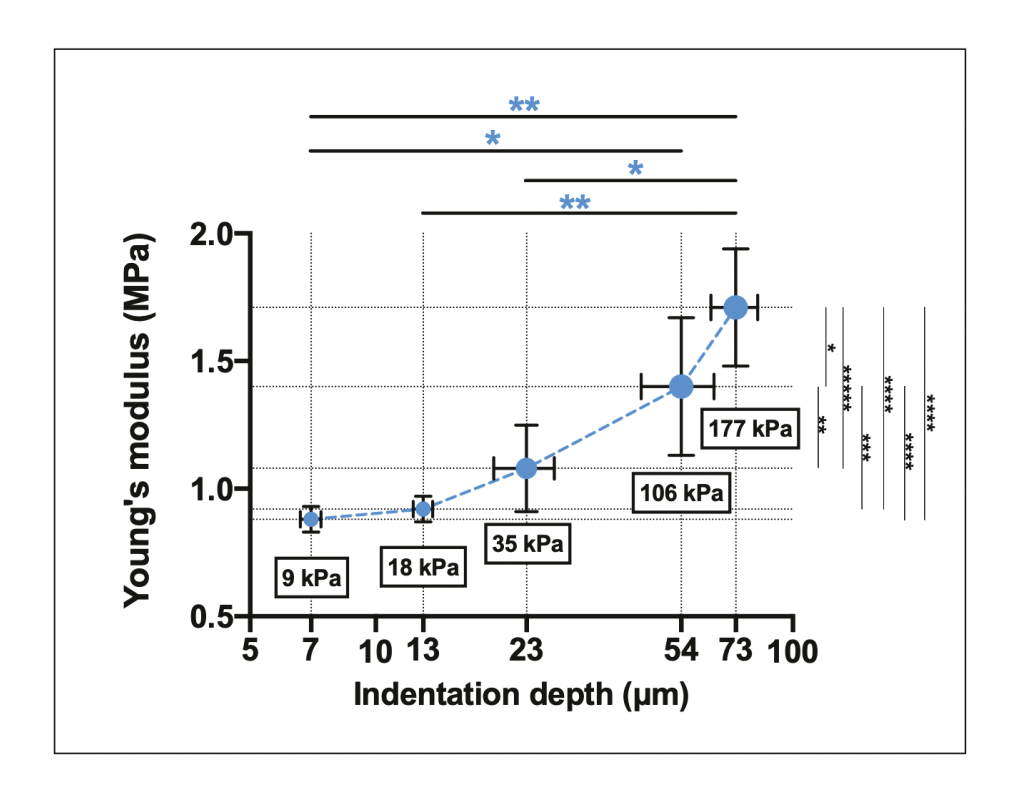


Figure S1. Change in the Young's modulus of the pHEMA (E_{pHEMA}) with respect to the increase in the indentation depth ($H_{steel-pHEMA}$) along with the increase in the contact pressure. Note that a base-10 log scale is used for the x-axis (indentation depth). The horizontal p-value (blue *, top of the figure) shows the significant difference amongst the values of E_{pHEMA} , and the vertical p-value (black *, right of the figure) shows the significant difference amongst the values of $H_{steel-pHEMA}$ (*: p < 0.05; **: p < 0.001; ***: p < 0.005; ***: p < 0.0001). The error bars in the graph represent standard deviations.

Table S2. Mechanical properties of a glass curve and pHEMA hydrogel

	Upper Fixed Object: Glass Curve	Lower Sliding Object: pHEMA
Radius of Curvature, R (mm)	30	∞ (i.e., flat)
Young's Modulus, E (MPa)	7.2×10^4	1.2 ± 0.1
Poisson's Ratio, v	0.2	0.5

Table S3. Average contact pressure, radius of contact area, and indentation depth in tribological experiments estimated based on the Hertzian contact theory.

Load, F (mN)	Average Contact Pressure, P (kPa)	Radius of Contact Area, r_{HC} (μ m)	Indentation Depth, H_{HC} (μ m)
6	10.0 ± 0.5	439 ± 12	6.5 ± 0.3
60	21.4 ± 1.2	946 ± 26	29.9 ± 1.7

EFFECT OF LOAD ON MATERIAL YOUNG'S MODULUS

Of note, since the solid area fractions of the micropored surfaces are greater than 50% ($\phi \ge 0.5$), the contact pressure on the micropored surfaces will increase no more than twice than that on the smooth surface at the given same load. When the microtextures are flattened out under the relatively high load, the difference in the contact pressure will be even much smaller. Although the Young's modulus of pHEMA increases with the contact pressure or indentation depth, the increase rate is quite modest. Based on the Young's modulus measured with smooth bulk pHEMA as shown in Table S1 and Figure S1, the increase in the Young's modulus with the contact pressure is less than two-fold (from 0.88 to 1.71 MPa) while the contact pressure and indentation depth increase about 20 times (from 9 to 177 kPa) and 10 times (from 7 to 73 µm), respectively. Thus, the Young's modulus of the micropored pHEMA films even with the lowest solid area fraction (i.e., $\phi = 0.5$) would not make a significant difference from that of the untextured smooth pHEMA film. Thus, the averaged Young's modulus value of 1.2 ± 0.1 MPa over the tested contact pressure range of 9 to 177 kPa was used to estimate the approximate values of the interfacial stiffness, the radius of a contact area, the average contact pressure, and the indentation depth for the Hertzian contact on both the untextured and micropored pHEMA films in the tribological experiments performed with a glass curve.

REAL-TIME VELOCITY PLOTS EXPORTED FROM UMT-3

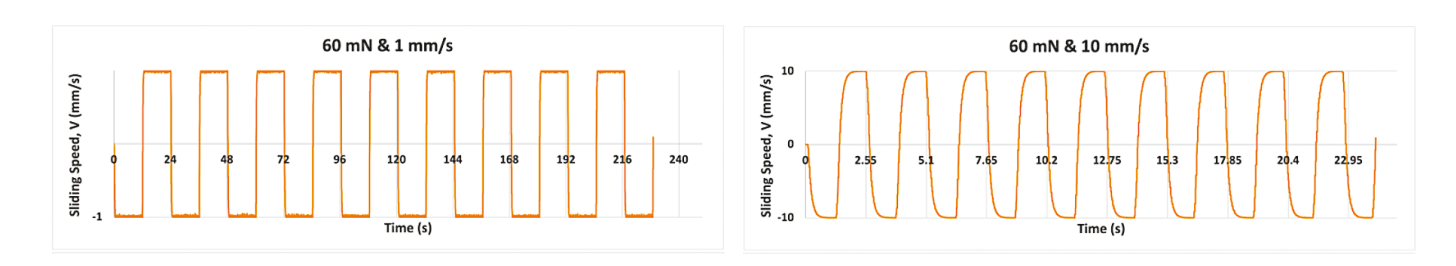


Figure S2. Examples of the change in sliding speed and friction force during 10 sliding cycles of the experiment where the glass curve slides against the untextured pHEMA surfaces with the sliding speed of 1 and 10 mm/s, respectively, under 60 mN.

ROUGHNESS OF A GLASS CURVE

According to the measurement by atomic force microscope, the roughness (R_a) of the glass curve is less than 5 nm, as shown in **Figure S3**.

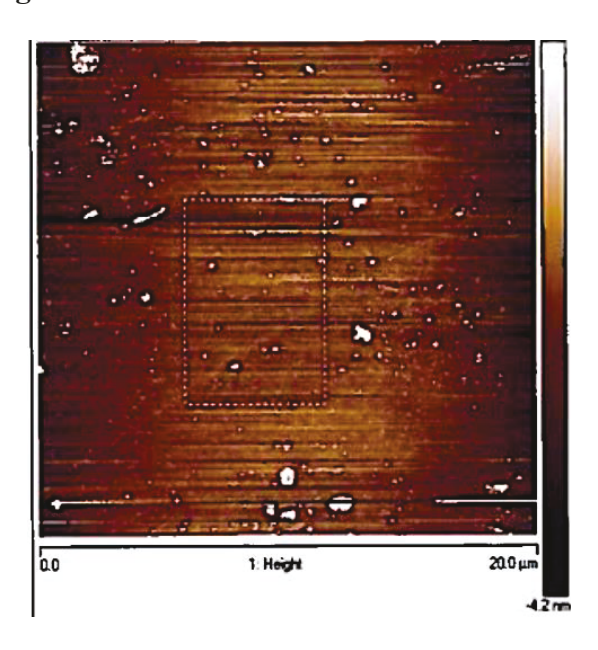


Figure S3. Atomic force microscope image of the glass curve surface of the area of 20 $\mu m \times 20 \mu m$.

RESULTS OF T-TEST ANALYSIS OF THE COF MEAN VALUES

Table S4. Results of *t*-test analysis of the COF mean values for the two different sliding speeds and loads, respectively (ns: not significant; *: p < 0.05; **: p < 0.001; ***: p < 0.0005; ***: p < 0.0001).

	Experimental	6 mN	60 mN	1 mm/s	10 mm/s
No.	Methods	1 vs. 10 mm/s	1 vs. 10 mm/s	6 vs. 60 mN	6 vs. 60 mN
1	$\phi = 1$	*	****	****	**
2	$\phi = 0.8, \ a = 3, \ b = 3$	*	****	****	ns
3	$\phi = 0.8, a = 6, b = 6$	*	****	****	ns
4	$\phi = 0.8, a = 12, b = 12$	**	****	****	ns
5	$\phi = 0.5, \ a = 3, \ b = 12$	*	****	***	ns

Table S5. Results of *t*-test analysis of the COF mean values of two different surfaces under the same load and speed (ns: not significant; *: p < 0.05; **: p < 0.001; ***: p < 0.0005; ****: p < 0.0001).

				6 mN		60 mN	
No.	Surface A	vs.	Surface B	1 mm/s	10 mm/s	1 mm/s	10 mm/s
(Untex	(Untextured vs. textured surfaces)						
1	$\phi = 1$	VS.	$\phi = 0.8, \ a = 3, \ b = 3$	****	ns	****	****
2	$\phi = 1$	VS.	$\phi = 0.8, \ \alpha = 6, \ b = 6$	****	ns	****	****
3	$oldsymbol{\phi}=1$	VS.	$\phi = 0.8, \ a = 12, \ b = 12$	****	ns	****	****
4	$oldsymbol{\phi}=1$	VS.	$\phi = 0.5$, $a = 3$, $b = 12$	**	ns	****	****
(Fixed	ϕ)						
5	$\phi = 0.8, \ a = 3, \ b = 3$	VS.	$\phi = 0.8, \ a = 6, \ b = 6$	****	ns	****	****
6	$\phi = 0.8, \ a = 3, \ b = 3$	VS.	$\phi = 0.8, \ a = 12, \ b = 12$	****	ns	****	****
7	$\phi = 0.8, \ a = 6, \ b = 6$	VS.	$\phi = 0.8, \ a = 12, \ b = 12$	**	ns	****	*
(Fixed a)							
8	$\phi = 0.8, a = 3, b = 3$	VS.	$\phi = 0.5, a = 3, b = 12$	****	ns	****	****
(Fixed b)							
9	$\phi = 0.8, \ a = 12, \ b = 12$	VS.	$\phi = 0.5, a = 3, b = 12$	****	ns	****	****

TIME-DEPENDENT RAW DATA OF NORMAL FORCE (F_Z) , FRICTION FORCE (F_X) AND COF VALUES

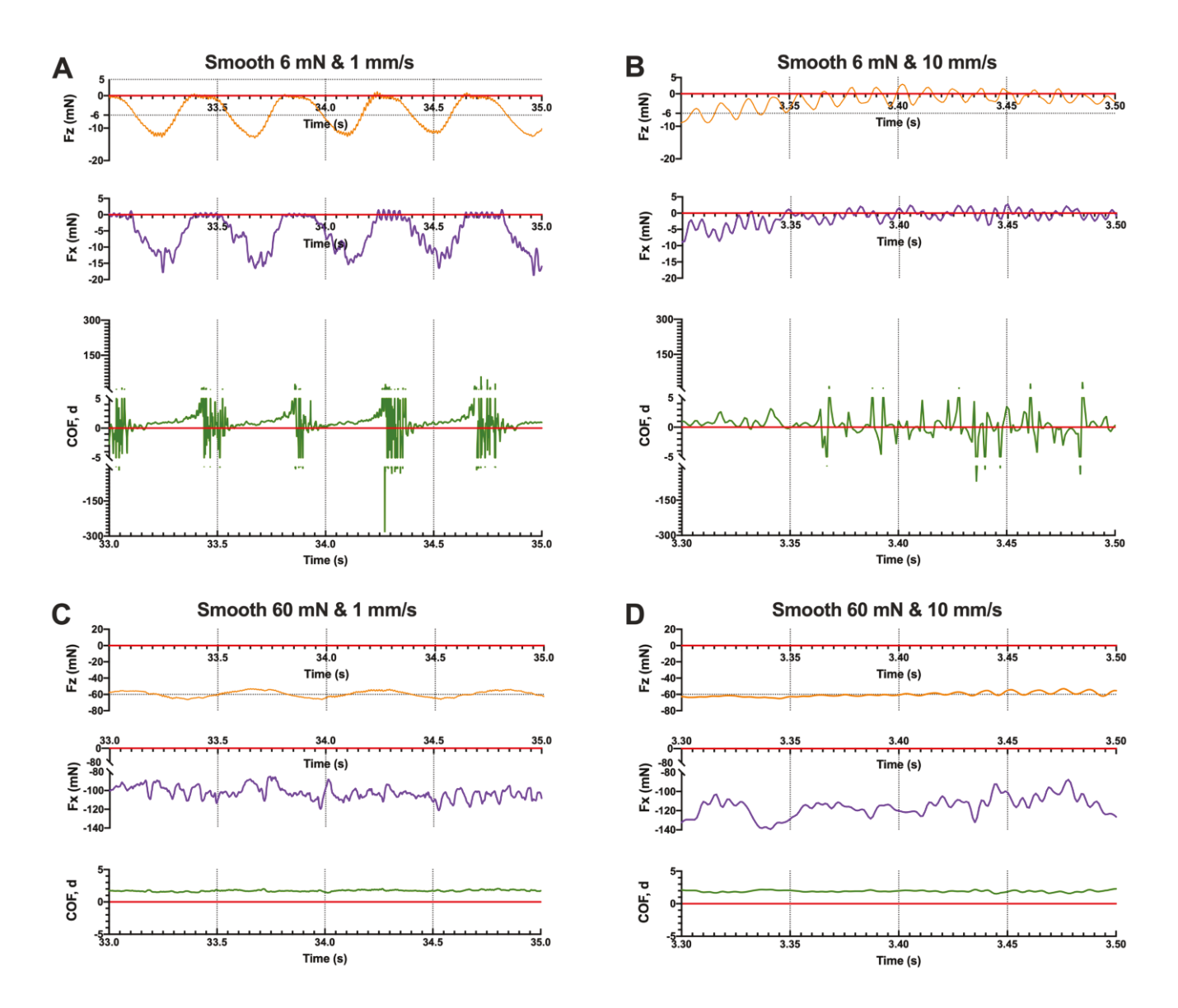


Figure S4. (A-D) Time-dependent tribological raw data for the smooth (untextured) pHEMA in terms of normal force (F_z) (orange), friction force (F_x) (purple) and COF (green) with the line of y = 0 highlighted by red. Only 1/6 period in the middle of the 2nd cycle is shown in each figure (i.e., about 4 s for 1 mm/s and 0.4 s for 10 mm/s).

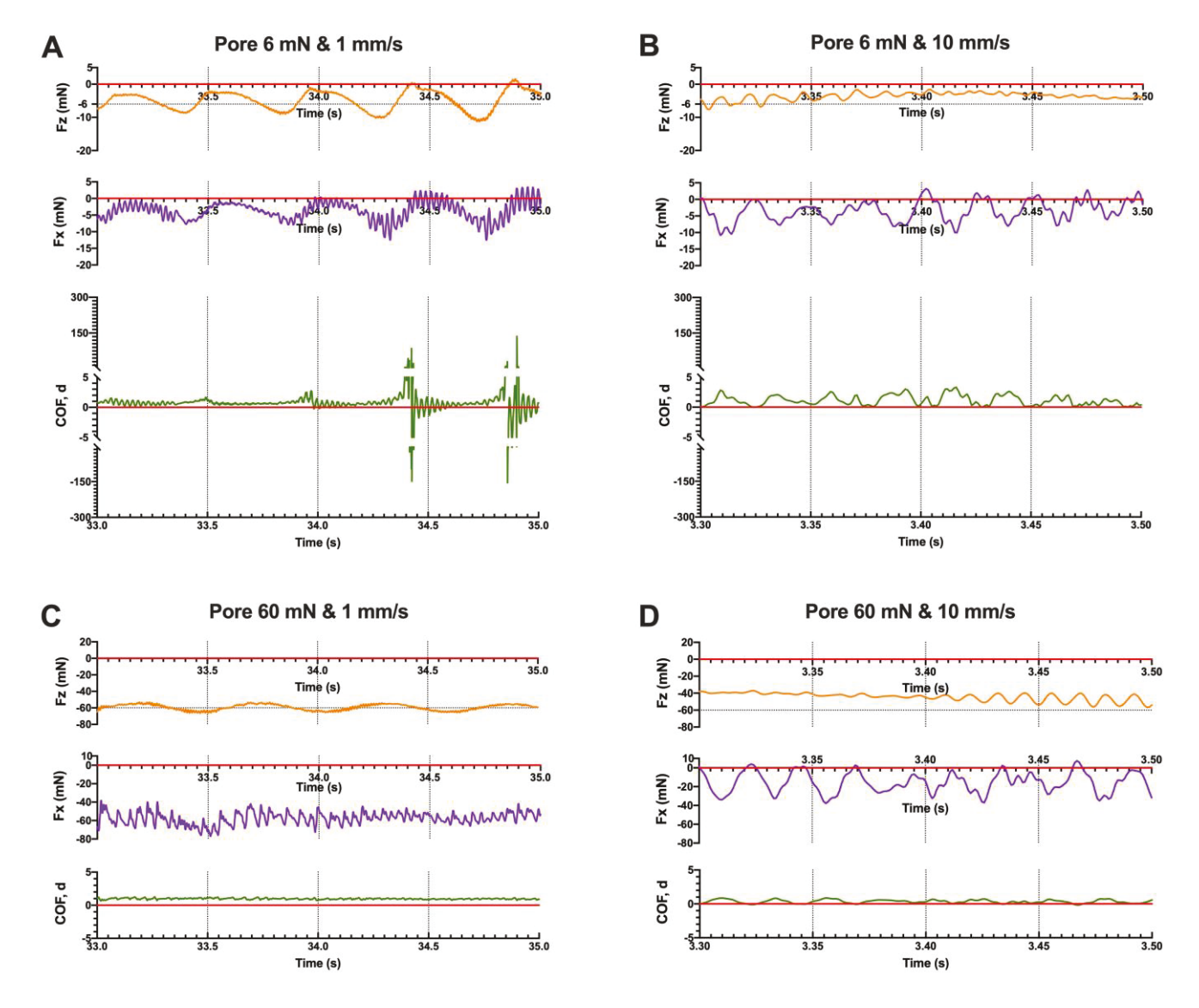


Figure S5. (A-D) Time-dependent tribological raw data for micropored pHEMA ($\phi = 0.5$, a = 3, b = 12) in terms of normal force (F_z) (orange), friction force (F_x) (purple) and COF (green) with the line of y = 0 highlighted by red. Only 1/6 period in the middle of the 2nd cycle is shown in each figure (i.e., about 4 s for 1 mm/s and 0.4 s for 10 mm/s).